Anomalous Transport in Disordered Dynamical Systems

G. Radons

Chemnitz University of Technology, Institute of Physics, D-09407 Chemnitz

Abstract

We consider simple extended dynamical systems with quenched disorder. It is shown that these systems exhibit anomalous transport properties such as the total suppression of chaotic diffusion and anomalous drift. The relation to random walks in random environments, in particular to the Sinai model, explains also the occurence of ageing in such dynamical systems. Anomalous transport is explained by spectral properties of corresponding propagators and by escape rates in these systems. For special cases we provide a connection to quantum mechanical tight-binding models and Anderson localization. New classes of anomalous transport behavior with clear deviations from the behavior of Sinai type are found for generalizations of these models.

Key words:
chaotic transport, chaos, disorder, random walks in random environments, Anderson localization, Sinai disorder
PACS: 05.45.-a, 02.50.-r, 05.40.-a, 05.60.-k, 46.65.+g

1 Introduction

Chaotic transport is nowadays a well established research field in nonlinear dynamics [1] [2] with applications in many branches of physics. Examples are ionization processes in atomic physics, tracer diffusion in hydrodynamics, or electron transport in solid state physics. Recently this field found renewed interest also from the fundamental point of view of non-equilibrium statistical mechanics. The key concepts for the characterization of such systems are spectra of Lyapunov exponents, various dynamical entropies, and fractal

Email address: radons@physik.tu-chemnitz.de (G. Radons).

dimensions of strange attractors or repellers in phase space and their connections with transport coefficients and escape rates [3] [4]. Most investigations considered systems where phase space or real space is infinitely extended with a continuous or discrete translational symmetry. The latter allows the reduction of the problem to a unit cell leading to compact phase spaces, typically a many-dimensional torus. Clearly these are limiting cases, and one wonders what happens for systems with broken translational invariance. In the following we treat examples, where order in this sense is not present, but the other extreme is prevailing, namely full disorder. Disordered systems are usually considered as a branch of statistical physics or solid state physics [5] with concepts and methods very different from the ones in dynamical systems theory. The model classes considered below, suggest that ageing phenomena and disorder induced anomalous transport are phenomena that arise very frequently also in disordered dynamical systems. We will also see how the above mentioned characteristics of dynamical systems reflect these disorder phenomena. The paper is organized as follows. In Section 2 we explain how chaotic diffusion is suppressed in dynamical systems defined by disordered iterated maps in one dimension and for area-preserving maps. In Section 3 it is argued that such systems exhibit phase-transition phenomena and that they are among the simplest to show non-trivial ageing behavior, a phenomenon which is usually studied in disordered many-particle systems. Section 4 provides insight into the anomalous transport properties through the spectral properties of corresponding propagators, thereby making also a connection to the escape rate formalism for dynamical systems. In special cases the problem is mapped to a quantum mechanical tight-binding model exhibiting Anderson localization. Finally, in Section 5 we introduce further extensions of the treated systems resulting in new classes of anomalous behavior and give some perspectives for future research.

2 Suppression of Chaotic Diffusion by Quenched Disorder

The simplest disordered dynamical systems are those with one or two degrees of freedom with disorder in the environment. An example is the Hamiltonian motion of a point particle in a two-dimensional disordered potential consisting of hard discs (Lorentz gas [6]) or smoothed version thereof. The periodic counterparts of these models have received much experimental and theoretical attention in connection with mesoscopic transport in quantum dot lattices [7] [8]. There in the spirit of [9] the importance of classical phase space structures and chaotic diffusion was realized [8]. Here we will concentrate first on dissipative systems which may also show chaotic transport. A simple much studied example is the damped motion of a periodically driven particle in a periodic potential. This provides e.g. a model for superionic conductors in an

external field and currently finds renewed interest in the context of ratchet physics. Simplified versions which are assumed to capture essential aspects of these systems are one-dimensional iterated maps [10]-[13]. While the periodicity in the equations of motion allows for the application of advanced methods such as periodic orbit theory, the thermodynamic formalism, or Levy flight statistics [16]-[22], it is clearly of much greater importance to understand the effects of static disorder in such systems. From the physics of disordered systems, it is known that static or quenched randomness may drastically alter macroscopic quantities such as transport coefficients. In the following we will first report on such an effect for dynamical systems, namely the total *suppression of normal or anomalous chaotic diffusion by quenched randomness* in the equations of motion. We will show that this can occur in both, dissipative and Hamiltonian systems. This turns out to be a non-trivial effect, since the mean-square displacement will remain finite, although chaotic transport is *not* inhibited locally.

2.1 One-dimensional iterated maps with disorder

Let us first concentrate on one-dimensional non-invertible maps of the type studied in [10]-[16]. They have the general form $x_{t+1} = f(x_t) = x_t + F(x_t)$, with $F(x)$ periodic in x. The periodicity interval, which we set equal to one, i.e. $F(x) = F(x+1)$, defines cells or half open intervals $A_i = [i, i+1), i \in \mathbb{Z}$, on the real axis. We will modify these dynamical systems by randomly changing $F(x)$ in each cell A_i to a function $F^{(i)}(x)$ resulting in

$$x_{t+1} = x_t + F^{(i)}(x_t) \tag{1}$$

for $x_t \in A_i$. This corresponds to a random variation in space of the driving force felt by the particle. A natural choice for $F^{(i)}(x)$ consists of random shifts of F

$$F^{(i)}(x) = F(x) + \epsilon(i). \tag{2}$$

In order to avoid complications connected with a global bias we assume for the moment the symmetry $F(-x) = -F(x)$, and further that the $\epsilon(i)$ are independent, identically distributed (i.i.d.) random variables with a symmetric distribution function $p(\epsilon) = p(-\epsilon)$ implying $\overline{\epsilon(i)\epsilon(j)} \propto \delta_{ij}$ and $\overline{\epsilon(i)} = 0$. Through the cell index i, defined as $i = [x]$, the largest integer smaller than x, the term $\epsilon(i)$ is recognized as piecewise constant random function of x. In contrast to previous studies [10], where time-dependent noise was added to the deterministic dynamics, the random term $\epsilon(i)$ remains constant in time, Eq.(1) is still deterministic, it describes a dynamical system with *quenched* randomness.

Fig. 1. (a) Simple piecewise linear maps corresponding to a periodic (dashed) and a random driving 'force' (bold). (b) The mean-square displacement $\sigma^2(t)$ increases linearly for the former (dashed line) and saturates in the latter case as shown for several disorder realizations (full lines: for $\epsilon(i) = \pm 1/2$, dot-dashed graphs: $\epsilon(i)$ equally distributed in $(-1/2, +1/2)$). There exist environments where a first constant level is observed only after more than $t = 10^6$ iterations ($0.5 \ldots 1.0 \times 10^7$ for the second graph from the top).

Let us now investigate the effect of this static randomness first for the simplest maps which in the absence of disorder ($\epsilon(i) = 0$) exhibit chaotic diffusion. These are systems where $F(x)$ varies linearly in each cell, i.e. $F(x) = a\{x\} - a/2$ with $\{x\} = x - [x]$. Since the slope of $f(x)$ is $a + 1$ these maps are chaotic for $a > 0$ and show chaotic diffusion for $a > 1$. The dashed graph in Fig.1(a) is an example with $a = 3$. The diffusive motion for this ordered case is verified by the linear increase of the mean-square displacement $\sigma^2(t) = \langle x_t^2 \rangle - \langle x_t \rangle^2 = 2Dt$ with the correct diffusion constant $D = 1/4$ [11] (dashed straight line in Fig.1(b)). This and the following results for $\sigma^2(t)$ were obtained numerically by iterating ensembles of 2×10^4 points (initially distributed homogeneously or inhomogeneously in one cell) for 10^6 (occasionally 10^7) time steps. An example of a map with binary disorder, $\epsilon(i) = \pm 1/2$ in Eq.(2), is shown as full line in Fig.1(a). Now, with disorder $\epsilon(i) \neq 0$, a very different behavior is observed: $\sigma^2(t)$ saturates and remains bounded for large times. As is seen from Fig.1(b) this is true for discrete random variations as well as for continuously distributed random variables $\epsilon(i)$. We emphasize that for both cases there exists no obvious reason why the spreading of the distribution $\rho(x, t)$ should be limited because the *a priory* probability for reaching one of the neighboring cells is always finite. More explicitly, *independent* of the chosen sequence $\epsilon(i)$, a fraction $p = 1/4$ of a homogeneous distribution in some cell A_i is always transferred to the right neighboring cell A_{i+1}, the same fraction to the left cell A_{i-1}, and one quarter remains within the cell A_i. From this point of view there is no difference between the homogeneous situation ($\epsilon(i) = 0$) and the inhomogeneous case ($\epsilon(i) \neq 0$). The randomness affects only the last quarter, which is mapped into one or both of the next-nearest cells $A_{i\pm 2}$. Note also that the degree of chaoticity as measured by the Lyapunov exponent (Fig.1: $\lambda = \ln 4$) is not altered by the random shifts.

The explanation of this localization effect in the case of quenched randomness follows from the following connection. For the map $f(x)$ with discrete random shifts $\epsilon(i) \in \{+1/2, -1/2\}$ as in Fig.1a), the cells A_i define a (generating) Markov partition [23][3][4]. This implies that the evolution of piecewise constant distributions $\rho(x,t)$ (constant in the cells A_i) is fully equivalent to a Markov process, i.e. the content $\pi_i(t) = \int_i^{i+1} \rho(x,t)\,dx$ of cell A_i at time t is iterated according to

$$\pi_j(t+1) = \sum_i \pi_i(t) p_{ij}. \tag{3}$$

For the above piecewise linear map with $\epsilon(i) = \pm 1/2$ the only non-zero transition probabilities p_{ij} are given by $p_{ii} = p_{i,i\pm1} = 1/4$ and $p_{i,i\pm2} = (1/2 \pm \epsilon(i))/4$. In the following we call this map of Fig.1(a) a *map with topological disorder*, because in the associated Markov model all non-zero transition probabilities are equal and thus the full information about the disorder is contained alone in the connectivity of the Markov model, or in technical terms, the adjacency matrix of the Markov process. The results of Fig.1 were also checked by iterating Eq.(3) with these transition probabilities. Such a model defines a discrete random walk in a locally asymmetric random environment. The above localization effect, i.e. $\sigma^2(t)$ remaining finite for $t \to \infty$, is known as *Golosov phenomenon* in the random walk literature [24]. Inspired by Sinai's work [25] it was proven rigorously for random systems with only nearest neighbor transitions by Golosov [26]. Reversing the above arguments which led us from iterated maps to random walks, it is obvious that also for the latter systems there exist realizations in terms of dynamical systems. These consist of piecewise linear chaotic maps of the form Eq.(1), with a typical example shown in Fig.2. Again the cells A_i provide a Markov partition for this system. The segments of length p_{ii} and $p_{i,i\pm1}$ in each unit cell, where the map $f(x)$ is linear, correspond to the non-zero transition probabilities p_{ii} and $p_{i,i\pm1}$ of the associated Markov chain.

The asymptotically finite mean-square displacement was proven in [26] for independent random sequences p_{ii} and $p_{i,i-1}/p_{i,i+1}$ with $\overline{\ln(p_{i,i-1}/p_{i,i+1})} = 0$. Maps with these properties will for further reference be called *maps with Sinai disorder*. The latter condition means that there is no global bias in the system and that one observes recurrent behavior with probability one.

So far we have seen that the dynamical systems defined in Fig.1 and Fig.2 both can be mapped to random walk models with (locally) asymmetric random transitions probabilities to next-nearest respectively nearest neighbors. An intuitive picture for the relevant physical processes is obtained from the continuum limit of the nearest neighbor discrete random walk model, which is Brownian motion in a spatially random force field $\tilde{F}(x)$ [24]. In this limit

Fig. 2. An example from the class of iterated maps for which the asymptotically finite mean-square displacement follows rigorously due the work of Sinai and Golosov [25] [26]. Also shown by dashed lines are the unit squares of the integer grid (see Fig.1(a)) along the bisectrix. The indicated intervals p_{ii} and $p_{i,i\pm1}$ mediate the transitions from the i-th cell A_i to itself and its neighbors respectively. They vary randomly from cell to cell.

the dynamics is governed by the Langevin equation

$$\dot{x}(t) = -\frac{\partial \tilde{V}}{\partial x}(x(t)) + \xi(t) \tag{4}$$

with Gaussian white noise $\xi(t)$. The important point is that the graph of the associated potential $\tilde{V}(x) = -\int^x \tilde{F}(x')dx'$ itself can be thought of as a realization of a Brownian path. The resulting statistical self-similarity of the potential $\tilde{V}(Lx) \simeq L^{1/2}\tilde{V}(x)$ implies the occurrence of deeper and deeper potential wells as the particle proceeds. The work of Sinai and Golosov shows that an ensemble of initially close particles moves in a coherent fashion from one deep minimum to the next deeper potential well. In this stepwise process it is *typically* one minimum which dominates and therefore determines the (finite) width $\sigma^2(t)$ of the ensemble [27] [28]. Since the random environment in the neighborhood of these minima is the same only in a statistical sense one observes for a fixed environment still fluctuations in $\sigma^2(t)$. These fluctuations become extremely rare for large times t as follows from an Arrhenius argument [24] which says that the typical time to overcome the ever increasing relevant potential barriers increases exponentially with the barrier height, i.e. it takes a time of the order $\exp(b\sqrt{x})$ for the state to travel a distance x. Solving this relation for x says that the typical distance reached in time t increases only as $\ln^2 t$. Indeed it has been shown rigorously that the mean displacement grows anomalously as

$$\langle x(t)\rangle = \xi(t)\ln^2 t \tag{5}$$

with $\xi(t)$ a random function of $O(1)$ [25][26][24]. By averaging over the environment this law is often expressed as

$$\overline{\langle x(t)\rangle^2} \sim \ln^4 t \tag{6}$$

often called "Sinai diffusion". A more rigorous review of Sinai's and related findings for random walks in random environments can be found in the monograph of Hughes [29].

Applying this picture of a thermally activated process in a random Brownian landscape to dynamical systems presupposes the existence of a Markov partition. The results of Fig.1 for continuous distributions of shifts $\epsilon(i)$, however, show that the observed localization phenomenon is not bound to the existence of a Markov partition. One may also expect that the feature of piecewise linearity is not necessary for the occurrence of this effect. Indeed we have shown in [30] that even anomalously enhanced diffusion generated by certain nonlinear maps where $F(x)$ varies sinusoidally in each cell [15], is totally suppressed by the introduction of disorder of the above type.

2.2 Disordered area-preserving maps

One may wonder whether this sort of dynamical localization can be observed also in Hamiltonian systems or area preserving maps. This question was answered affirmatively by the explicit construction of an area preserving map of the baker type, which shows the same behavior [31]. The resulting inhomogeneous chain of baker maps is a generalization of a class of dynamical systems (homogeneous chains of baker maps), which recently became very popular (see [4], and refs. therein) and which were originally introduced by Hopf in [32]. The construction is shown in Fig.3 below.

Fig. 3. The construction of an area-preserving inhomogeneous chain of baker maps, which in the projection on the x-axis reveals exactly the dynamics of the one-dimensional iterated map of Fig.2.

It consists of an array of L rectangles called cells $A_i, i = 0, \ldots, L-1$, of unit width in the $x-$direction and heights π_i. During one iteration step the inscribed rectangles within one cell A_i are mapped to the neighboring cells and into the present cell as follows: Take e.g. the black rectangle of height π_i and width $p_{i,i-1}$, which is labeled by its area $\pi_i p_{i,i-1}$ in Fig.3. This rectangle is in one iteration (from top to bottom in Fig.3) squeezed in the $y-$direction, stretched in the $x-$direction, and transferred to the left neighboring cell A_{i-1}in an area preserving manner. In the same way the grey-shaded rectangle $\pi_i p_{i,i+1}$ is transferred to the right, and the light-grey rectangle gets squeezed and stretched, but remains in the cell A_i as shown in the figure. For a finite chain we may impose periodic boundary conditions $A_{i+L} = A_i$ ($L = 3$ in Fig.3), or, alternatively one could confine transport within the array by appropriate modifications of the boundary maps ($p_{0,-1} = p_{L-1,L} = 0$). Analogously one can define an infinitely long chain of baker maps, and one observes that the $x-$coordinate x_t of a point (x_t, y_t) in this two-dimensional area preserving map is iterated exactly as a point x_t of the one-dimensional map of Fig.2 (with slopes $p_{i,j}^{-1}$). This implies that the dynamical localization phenomenon of the previous section is found also in these area preserving maps.

Note, however, that in order to get an area preserving map, the heights π_i have to be adjusted appropriately. The condition that in one iteration the outflow of area of a given cell, say A_i, has to be equal to its inflow, results in

$$\pi_{i-1} p_{i-1,i} + \pi_{i+1} p_{i+1,i} = \pi_i p_{i,i-1} + \pi_i p_{i,i+1}. \tag{7}$$

Adding to both sides of this equation the term $\pi_i p_{i,i}$ and using the normalization $\sum_j p_{i,j} = 1$, one finds that the π_i fulfill the equation for the stationary probability distribution of a Markov chain with transition probabilities $p_{i,j}$. The latter exists for random $p_{i,j}$ only if the system is finite. For reflecting boundary conditions this stationary distribution can be found exactly as

$$\pi_i = \pi_0 \prod_{k=0}^{i-1} \frac{p_{k,k+1}}{p_{k+1,k}}. \tag{8}$$

For periodic boundary conditions a similar result is obtained [33] [34]. A characterization of such stationary distributions in terms of its cumulants was given recently in [35]. There is no need to restrict one-self to finite chains. Imposing for the infinite system the condition that the flow of area in one iteration from cell A_i to cell A_{i+1} is equal to the backflow from A_{i+1} to A_i implying a vanishing net current through the system, one obtains as condition for the heights π_i

$$\pi_i p_{i,i+1} = \pi_{i+1} p_{i+1,i} \tag{9}$$

which has to hold for all i. The solution of this infinite system of equations is for $i > 0$ given again by Eq.(8) and an analogous expression holds for $i < 0$.The cell label A_0 can be attached to some arbitrarily chosen cell, and the height π_0 is an arbitrary constant. Only for finite systems one can assign to the heights π_i the meaning of a stationary distribution, and Eq.(9) then becomes the condition for detailed balance, which is automatically fulfilled in the case with reflecting boundary conditions. For quenched random transition probabilities, as in the models treated here, Eq.(9) means that the π_i follow a random multiplicative process as given by Eq.(8), which occur naturally in many branches of physics. Of course it would be of interest whether for some class of area preserving maps or corresponding continuous time Hamiltonian systems, such a distribution of chaotic areas occurs naturally. In such cases one expects that one finds the same anomalous transport properties as in the simple maps introduced here. This will be observable until the boundaries of the system of size L are reached, which for extended systems occurs only at exponentially large times, i.e. at times of the order $O(\exp b\sqrt{L})$.

3 Phase Transitions and Ageing in Disordered Dynamical Systems

In this section we will point out that in the presence of a global bias the systems treated above show various *phase transitions* characterized by *anomalous chaotic transport* properties. Finally we argue that these systems can also show the phenomenon of *ageing*.

3.1 Phase transitions in biased systems

Releasing the conditions $\overline{\epsilon(i)} = 0$ for the system of Fig.1 or $\overline{\ln(p_{i,i-1}/p_{i,i+1})} = 0$ for that of Fig.2 leads us from systems without global bias to such with a bias. The latter may simulate an external static field or may be attributed to systematic asymmetries of the underlying potential in more realistic models, such as driven damped particles in some potential landscape. Such aspects are clearly of great importance in the context of transport in ratchets [36][37]. Although the connection between the simplified one-dimensional maps and more realistic models is complicated and not fully understood, the investigation of the former with bias will provide some insight into the possible scenarios in the latter.

Exploiting again the connection between maps and discrete time Markov chains, allows us to apply known results from the literature to disordered iterated maps. Analytical results by Derrida and Pomeau [33][34] for the biased case $\overline{\ln(p_{i,i-1}/p_{i,i+1})} \neq 0$ lead to transport properties for the corresponding

dynamical systems, which we summarize in Fig.4 for a special example of the type of Fig.2.

Fig. 4. The dependence of the normalized transport coefficients D/D_0 (bold) and V/V_0 (dashed) is shown as function of the defect concentration c. In the regimes where these are finite they are self-averaging quantities and therefore these values are observed with probability one independent of the disorder realization.

The example consists of setting $p_{ii} = 0$ and choosing a binary distribution for the transition probabilities $p_{i,i\pm1}$ of Fig.2. More explicitly, we construct a chain of maps consisting of two sorts of cells (see Fig.2), which we denote as A_+ and A_-. For the type A_+ we choose $p_{i,i+1} = a$ and correspondingly $p_{i,i-1} = 1 - a$, while for type A_- we reverse the assignments, i.e. we set $p_{i,i+1} = 1 - a$ and $p_{i,i-1} = a$. These cells are concatenated randomly and independently so that type A_+ is present in a concentration c and correspondingly a fraction $1 - c$ of cells are of type A_-. For Fig.4 we have chosen $a = 1/3$ so that for $c = 0$ we have an ordered system consisting only of cells A_-, which map points with larger probability, namely with probability $2/3$, to the right, and with probability $1/3$ to the left. In this limit one gets chaotic diffusion with a mean drift to the right, where diffusion constant D and drift velocity V are given by $D = D_0 = 2a(1 - a)$ and $V = V_0 = 1 - 2a$, respectively. The behavior of the transport coefficients, normalized by its bare values D_0 and V_0, is shown in Fig.4 as function of the concentration c. We need to discuss only the case $0 \leq c \leq 1/2$, since the rest follows by symmetry. For the other extreme of full disorder $c = 1/2$ we get the unbiased situation $\overline{\ln(p_{i,i-1}/p_{i,i+1})} = 0$, where the anomalous Sinai and Golosov results of section 2.1 hold. This means we get in this case $D = 0$ and $V = 0$. Between these extremes various transitions between dynamically different phases occur. In Fig.4 these different regimes are numbered as I-IV. In phase I both D and V are finite and non-zero, i.e. one has normal chaotic transport as in the ordered limit. The transition to phase II occurs at concentrations where conditions $\overline{(p_{i,i-1}/p_{i,i+1})^{\pm 2}} = 1$ are fulfilled (two symmetric solutions in c) . This transition is accompanied by D becoming infinite, which holds in regimes II an III. In these phases one has therefore anomalously enhanced diffusion, i.e. the mean-square displacement grows superlinear. The transition between II an III is signaled by a vanishing drift velocity, i.e. the mean displacement grows slower than linearly in time. The transition points are given by $\overline{(p_{i,i-1}/p_{i,i+1})^{\pm 1}} = 1$. The anomalously slow growth of the displacement holds up to the value $c = 1/2$, i.e. also in regime

IV. The transition from III to the latter is characterized by a crossover from superdiffusive to subdiffusive chaotic transport implying that in addition to V also D vanishes. The last transition is observed for $\overline{(p_{i,i-1}/p_{i,i+1})^{\pm 1/2}} = 1$. The fact that the qualitative changes in the drift and diffusion properties occur at different values of the concentration is quite common in disordered systems and is expected to hold also more generally. A more extensive description and a discussion of the different regimes in terms of activated Brownian motion in tilted Brownian potentials can be found in the review article [24]. Interestingly the same conclusions were reached very recently in the context of disordered ratchets by a totally different reasoning within a continuous time model [37]. Finally note that dynamical phase transitions as a consequence of an applied bias may also arise in ordered dynamical systems [38].

3.2 Ageing

The phenomenon of ageing is a well-known experimental fact from glasses, spin glasses, and other complex materials[39][40]. Theoretical investigations are also mainly concerned with these systems (see e.g. [41]-[43], and refs. therein), but recently ageing was found also in much simpler model systems [44][45]. Ageing can be defined as an anomalous behavior of response and correlation functions. Consider e.g. the correlation function $C_{AB}(t, t_w) \equiv \langle A(t_w)B(t + t_w)\rangle$ of two variables A and B, where t_w is the waiting time after the preparation of the initial state at time $t = 0$. For $t \ll t_w$ the correlation function $C_{AB}(t, t_w)$ is independent of t_w and a fluctuation-dissipation theorem is supposed to hold. Ageing is present if $C_{AB}(t, t_w)$ depends strongly on t_w when t is of the same order as t_w. Furthermore for t and t_w large one often assumes a scaling behavior of the form

$$C_{AB}(t, t_w) = t^{-\nu} F(\frac{t}{t_w}). \tag{10}$$

First numerical investigations by Marinari and Parisi [44] for random walks in random environments of Sinai type indicated a dependence $C_{AB}(t, t_w) = \ln^2(\frac{t}{t_w})$, i.e. $\nu = 0$ in Eq.(10) for various correlation functions. Recently, however, improved numerical simulations revealed a more complex behavior i.e. one finds asymptotically different logarithmic scalings depending on the ratio $\ln t/\ln t_w$ as t and t_w are sent to infinity [46]. The latter kind of scaling behavior was subsequently confirmed also analytically by an exact real space renormalization group (RSRG) calculation [47] [48]. In any case non-trivial ageing is found in random walks in random environments of Sinai type. As pointed out above such systems can be implemented by dynamical systems as introduced in Fig.2. This implies that ageing occurs also in these simple disordered dynamical systems and its generalizations treated in section 2.1. This

fact has been realized only recently [31]. We should remark that a behavior as in Eq.(10) is observed also in much simpler non-equilibrium systems, even without disorder: It was pointed out in [49] that already the simple homogeneous, one-dimensional random walk $\dot{x}(t) = \xi(t)$, i.e. the system governed by the Langevin equation, Eq. (4), without drift term, gives rise to a violation of the fluctuation-dissipation theorem and a scaling behavior for $C_{xx}(t, t_w)$ as in Eq.(10). The scaling, however, is trivial in this case, since $C_{xx}(t, t_w) = t_w$ implying $\nu = -1$ and $F(x) = 1/x$ in Eq.(10). It follows that the same simple scaling behavior applies also to dynamical systems, which lead to simple diffusion, e.g. the iterated maps in [10]-[13]. Note, however, that already in these simple iterated maps the scaling function depends in a non-trivial (fractal) manner on the parameters of the map. This a consequence of the fractal dependence of the diffusion coefficient on the system parameters [21]. A less trivial ageing behavior was found very recently [50] for periodic iterated maps leading to anomalous diffusion, especially in the systems introduced in [14]. Similar to the disordered case one finds in such systems a broad distribution of trapping times which can be related to the ageing property. In periodic iterated maps, however, the trapping is associated with marginally stable fixed points of the dynamics. Generalizations of this class of maps can exhibit in addition an extremely slow, i.e. a logarithmic increase in time of the mean square displacement [51], which is reminiscent of "Sinai diffusion", Eq.(6). Also for these maps one expects non-trivial ageing. We close this section with two remarks. First note that very recently many more exact results have been obtained for the Sinai model and its ageing properties, especially in the presence of a bias [52]-[56]. These results are valid also for the associated dynamical systems of Sinai type, but its applicability to more general dynamical systems is an open question. Secondly, questions arising in the context of aging of the validity of linear response and the fluctuation-dissipation theorem are well understood for stochastic systems as described by Langevin or Fokker-Planck equations (for disordered systems of Sinai type see [48]). Its applicability to general nonlinear dynamical systems, however, is still an active field of research despite the fact that first works in that direction appeared two decades ago [57] [58]. For the current status of this question see e.g. [59] [60] and refs. therein. In summary, the recent finding that simple ordered or disordered extended dynamical systems lead to ageing, raises important questions for future research, e.g. whether and how the different kinds of scaling behavior are related to different classes of dynamical systems.

4 Spectral Characteristics and Escape Rates

In this section we will provide a complementary view on the above results, as they are reflected in the spectral characteristics of the corresponding Frobenius-

Perron operator and associated transition matrices, respectively. For maps of the form $x_{t+1} = f(x_t)$ the Frobenius-Perron operator $\mathcal{P}$ describes the evolution of densities in phase space as $\rho(x, t+1) = \mathcal{P}[\rho(x,t)] = \int dy\, \rho(y,t)\, \delta(f(y) - x)$ [1] [4]. In the following we study the spectral properties of $\mathcal{P}$, i.e. its eigenvalues $\lambda^{(\alpha)}$ and eigenvectors $v^{(\alpha)}(x)$ given by

$$\mathcal{P}[v^{(\alpha)}(x)] = \int dy\, v^{(\alpha)}(y)\, \delta(f(y) - x) = \lambda^{(\alpha)} v^{(\alpha)}(x). \tag{11}$$

The spectral properties of $\mathcal{P}$ depend strongly on the function space considered. In the following we restrict ourselves to piecewise linear maps, for which the intervals $[i, i+1]$ provide a Markov partition (as in Figs. 1 and 2), and we consider the evolution of densities $\rho(x,t)$, which are constant in these intervals, i.e. $\rho(x,t) = \pi_i(t)$ for $x \in A_i = [i, i+1]$. For these maps this is not a strong restriction since sufficiently smooth initial densities $\rho(x,0)$ approach such a form exponentially fast. The evolution equation for the $\pi_i(t)$ is then given by Eq.(3). Correspondingly we investigate the spectral properties of $\mathcal{P}$ in the space of piecewise constant functions, where Eq.(11) can be replaced by

$$\sum_i v_i^{(\alpha)} p_{ij} = \lambda^{(\alpha)} v_j^{(\alpha)}. \tag{12}$$

The elements p_{ij} of the Markov transition matrix $\mathbf{P}$ are given by

$$p_{ij} = (\mathbf{P})_{ij} = 1/\left|f'_{i,j}\right| \tag{13}$$

with $f'_{i,j}$ denoting the derivative of that branch of $f(y)$ in the interval $A_i = [i, i+1]$, which maps points onto the interval A_j. For systems with a finite number L of cells A_i this implies that the invariant density $\rho^*(x) = \rho(x, t \to \infty)$, i.e. the eigenfunction of $\mathcal{P}$ with eigenvalue $\lambda = 1$, takes the form $\rho^*(x) = \pi_i$ for $x \in [i, i+1]$. The vector $\boldsymbol{\pi}$ with components $(\boldsymbol{\pi})_i = \pi_i$ is thus the left-eigenvector $\mathbf{v}^{(1)}$ of the $(L \times L)$ transition matrix $\mathbf{P}$ with eigenvalue $\lambda^{(1)} = 1$. The corresponding right-eigenvector is given by $\mathbf{u}^{(1)} = \boldsymbol{\eta} = (1, 1, \ldots, 1)$, expressing that $\mathbf{P}$ is a stochastic matrix, $\mathbf{P}\,\boldsymbol{\eta} = \boldsymbol{\eta}$. More generally we consider the spectral decomposition of $\mathbf{P}$ given by

$$p_{ij} = \sum_{\alpha=1}^{L} u_i^{(\alpha)} \lambda^{(\alpha)} v_j^{(\alpha)} \tag{14}$$

with $\{\mathbf{v}^{(\alpha)}\}$ and $\{\mathbf{u}^{(\alpha)}\}$ denoting the complete bi-orthonormal set of left- and right-eigenvectors of the transition matrix $\mathbf{P}$, i.e. $\mathbf{v}^{(\alpha)}\mathbf{P} = \lambda^{(\alpha)}\mathbf{v}^{(\alpha)}$ and $\mathbf{P}\mathbf{u}^{(\alpha)} = \lambda^{(\alpha)}\mathbf{u}^{(\alpha)}$ with $\mathbf{v}^{(\alpha)} \cdot \mathbf{u}^{(\beta)} = \delta_{\alpha\beta}$. Since $\mathbf{P}$ is a stochastic matrix all eigenvalues $\lambda^{(\alpha)}$ lie within the unit circle $\left|\lambda^{(\alpha)}\right| \leq 1$ according to the Perron-

Frobenius Theorem [61]. With the aid of Eq.(14) and the bi-orthonormality condition the evolution of $\pi_j(t)$ can be written as

$$\pi_j(t) = \sum_{i=1}^{L} \sum_{\alpha=1}^{L} \pi_i(0)\, u_i^{(\alpha)} \exp(-\epsilon^{(\alpha)} t)\, v_j^{(\alpha)}, \tag{15}$$

where we have introduced the (in general complex) relaxation rates $\epsilon^{(\alpha)}$ by setting $\lambda^{(\alpha)} = \exp(-\epsilon^{(\alpha)})$, with $\mathrm{Re}(\epsilon^{(\alpha)}) \geq 0$ and $-\pi < \mathrm{Im}(\epsilon^{(\alpha)}) \leq \pi$. Note that for $\lambda^{(\alpha)} \to 1$, i.e. $\epsilon^{(\alpha)} \to 0$ we can write $\epsilon^{(\alpha)} \approx 1 - \lambda^{(\alpha)}$.

4.1 Maps with Sinai disorder

Let us first consider the spectrum $\left\{\lambda^{(\alpha)}\right\}$ for dynamical systems with Sinai disorder as in Fig.2. It turns out that the eigenvalues $\lambda^{(\alpha)}$ are real in this case. The spectrum $\left\{\lambda^{(\alpha)}\right\}$, which is shown in Fig. 5 was obtained for a dynamical system of $L = 1000$ cells of the type of Fig.2, with the $\{p_{i,i-1}\}$ chosen randomly and with equal probability from $\{1/9, 8/9\}$, $p_{i,i} = 0$, and $p_{i,i+1} = 1 - p_{i,i-1}$ (Sinai disorder) and reflecting boundary conditions.

Fig. 5. The spectrum of a dynamical system of Sinai type. The eigenvalues apparently cluster near $\lambda = 1$ (and by symmetry also at $\lambda = -1$). They were obtained by numerically diagonalizing the transition matrix $\mathbf{P}$.

The importance and the meaning of the observed clustering in Fig.5 becomes apparent by considering the evolution of initial distributions $\rho(x, 0)$, which are constant in some cell $[k, k+1]$, i.e. $\pi_i(0) = \delta_{i,k}$ and to observe the time course of the probability in the initial cell $\pi_k(t)$. The latter is given by $\pi_k(t) = \sum_{\alpha=1}^{L} u_k^{(\alpha)} \exp(-\epsilon^{(\alpha)} t)\, v_k^{(\alpha)}$. Averaging this expression, i.e. the return probability, over all such initial conditions, one obtains $\langle \pi_k(t) \rangle \equiv \frac{1}{L} \sum_{k=1}^{L} \pi_k(t) = \frac{1}{L} \sum_{k=1}^{L} (\mathbf{P}^t)_{kk} = \frac{1}{L} \sum_{\alpha=1}^{L} \exp(-\epsilon^{(\alpha)} t)$, where in the last step we have used $\mathbf{v}^{(\alpha)} \cdot \mathbf{u}^{(\alpha)} = 1$. Introducing the density of relaxation rates

$$\rho(\epsilon) \equiv \frac{1}{L} \sum_{\alpha=1}^{L} \delta(\epsilon - \epsilon^{(\alpha)}) \tag{16}$$

one can express $\langle \pi_k(t) \rangle$ as the Laplace transform of $\rho(\epsilon)$, i.e.

$$\langle \pi_k(t) \rangle = \int_0^\infty d\epsilon \, \rho(\epsilon) \, \exp(-\epsilon t). \tag{17}$$

This quite general and well-known relationship shows that the decay process at the starting cell in the long time limit is determined by the small$-\epsilon$ behavior of $\rho(\epsilon)$, or, equivalently by the eigenvalues $\lambda^{(\alpha)}$ of $\mathbf{P}$ near $\lambda = 1$.

To obtain a better understanding of the spectrum $\{\lambda^{(\alpha)}\}$ of $\mathbf{P}$, we will show how this eigenvalue problem can be mapped to an equivalent quantum mechanical problem. Note first that $\mathbf{P}$ is a tridiagonal matrix. Such a matrix can always be transformed to a symmetric tridiagonal matrix $\mathbf{H}$ by a similarity transformation $\mathbf{S}$, i.e. one can write $\mathbf{P} = \mathbf{S}^{-1}\mathbf{H}\,\mathbf{S}$. One easily verifies that the matrix elements of $\mathbf{H}$ are given by $H_{i,i+1} = H_{i+1,i} = (p_{i,i+1}\, p_{i+1,i})^{1/2}$, $H_{i,i} = p_{i,i}$, and the matrix elements $S_{ij} = s_i \delta_{ij}$ of $\mathbf{S}$ fulfill the recursion relation $s_{i+1} = s_i \, (\, p_{i,i+1}/p_{i+1,i})^{1/2}$. A comparison with Eq.(9) and Eq.(8) shows that for finite L the matrix elements S_{ii} can be identified with $s_i = (\, \pi_i)^{1/2}$. Clearly the spectrum $\{\lambda^{(\alpha)}\}$ of $\mathbf{H}$ is identical with that of $\mathbf{P}$. Since $\mathbf{H}$ is symmetric, the $\lambda^{(\alpha)}$ are real as stated above. The eigenfunctions $\mathbf{\Psi}^{(\alpha)}$ of $\mathbf{H}$ can also be chosen real and are related to those of $\mathbf{P}$ by

$$u_i^{(\alpha)} = \Psi_i^{(\alpha)}/s_i, \;\; v_i^{(\alpha)} = \Psi_i^{(\alpha)} s_i. \tag{18}$$

The eigenvalue problem $\mathbf{H}\,\mathbf{\Psi}^{(\alpha)} = \lambda^{(\alpha)}\,\mathbf{\Psi}^{(\alpha)}$ can be regarded as a Schrödinger equation for the 1-d Anderson problem with tight-binding Hamiltonian $\mathbf{H}$ (see e.g. [62]). Note that the transformation of a 1-dimensional random walk problem to a quantum mechanical system is a standard procedure in the continuum limit [63], where the state dynamics is described by a Langevin equation as in Eq.(4) and the evolution of densities by the corresponding Fokker-Planck equation. In our case the problem is mapped to a 1-d Anderson Hamiltonian with on-site disorder, given by the elements $H_{i,i} = p_{i,i}$, and with off-site disorder by the hopping elements $H_{i,i+1} = H_{i+1,i} = (p_{i,i+1}\, p_{i+1,i})^{1/2}$. Note that although the $\{p_{i,i+1}\}$ are independent random variables, the $\{H_{i,i+1}\}$ are not independent due to the applied transformation, i.e. $\overline{H_{i,i+1}\, H_{i+1,i+2}} \neq \overline{H_{i,i+1}}\;\overline{H_{i+1,i+2}}$. Thus the off-site disorder is correlated. Since one knows that for such 1-d Anderson problems almost all eigenfunctions are exponentially localized, one would naively expect that in the corresponding random walk problem there will be no transport at all. This, however, is not true since the ground state $\mathbf{\Psi}^{(1)}$ is extended. We call $\mathbf{\Psi}^{(1)}$ a ground state because the relaxation rates $\epsilon^{(\alpha)} = 1 - \lambda^{(\alpha)} \geq 0$ are the eigenvalues of the Hamiltonian $\mathbf{1} - \mathbf{H}$ and $\mathbf{\Psi}^{(1)}$ corresponds to the lowest lying eigenvalue $\epsilon^{(1)} = 0$ of that Hamiltonian. To see that $\mathbf{\Psi}^{(1)}$ is extended in the limit $L \to \infty$, note that from Eq.(18) it follows

that $\Psi_i^{(1)} = (\pi_i)^{1/2}$. As mentioned above, the $\{\pi_i\}$ are given by a random multiplicative process with diverging fluctuations for $L \to \infty$, so that $\mathbf{\Psi}^{(1)}$ is not normalizable in that limit. This implies that the anomalous transport properties of the dynamical system with Sinai disorder are related to the spectral properties of $\mathbf{1} - \mathbf{H}$ near $\epsilon = 0$ (or, equivalently to that of $\mathbf{P}$ near $\lambda = 1$). In order to investigate quantitatively the clustering of eigenvalues near the ground state one best considers the integrated density of states (i.e. relaxation rates) defined by

$$N(\epsilon) = \int_0^\epsilon d\epsilon' \rho(\epsilon') \tag{19}$$

where $\rho(\epsilon)$ is given by Eq.(16) with $\epsilon^{(\alpha)} = 1 - \lambda^{(\alpha)}$. Fig.6a) shows $N(\epsilon)$ on a linear scale for the spectrum of Fig.5. $N(\epsilon)$ increases monotonically from 0 to 1, and appears to be singular near $\epsilon = 0$. This singular behavior is confirmed in Fig.6b), where we plot N vs. $|\ln \epsilon|$ on a doubly logarithmic scale.

Fig. 6. a) The density of states $N(\epsilon)$ corresponding to the spectrum of Fig.5. b) The singular behaviour is confirmed in a log-log plot of $N(\epsilon)$ vs. $|\ln \epsilon|$. The dashed line corresponds to a dependence $\widetilde{N}(\epsilon) = 2/\ln^2 \epsilon$

The asymptotic behavior of $N(\epsilon)$ for $\epsilon \to 0$ which is given by the dashed line corresponds to

$$\widetilde{N}(\epsilon) = c/\left|\ln \epsilon\right|^\delta \tag{20}$$

with $c = 2$ and $\delta = 2$. Thus $\rho(\epsilon)$ diverges at the band edge as $4/(\epsilon \left|\ln \epsilon\right|^3)$. This analytic form of $\widetilde{N}(\epsilon)$ was obtained by Bouchaud et al. [64] for an exactly solvable continuum model for a random walk in a random environment, which has the same asymptotics as the continuum model of the Langevin equation Eq.(4). For the latter the logarithmic divergence of $\widetilde{N}(\epsilon)$ was already observed numerically in [65]. A similar divergence is known for the Dyson model of localization [62]. Our results of Fig.6 imply that the discrete state, discrete time random walk model has the same asymptotics as the continuum model. For our dynamical system with Sinai disorder, Fig.2, this means that the long time behavior of $\langle \pi_k(t) \rangle$ is given by Eq.(17) resulting in $\langle \pi_k(t) \rangle \sim 2/\ln^2 t$ for

long times. This fits very well into the picture that the decay at some initial cell k is caused by the anomalous drift $\langle x(t)\rangle = O(\ln^2 t)$, Eq.(5). More accurately this statement is captured in the generally accepted scaling assumption $\overline{(P^t)_{kl}} = \frac{1}{y(t)} g(\frac{x}{y(t)})$ with $x = |k-l|$ (see e.g. [66]). Setting $x = 0$ and assuming that self-averaging holds, i.e. by replacing the average over all cells $\langle \pi_k(t)\rangle$ by the disorder average $\overline{\pi_k(t)}$, it follows that $y(t) = \ln^2 t$. From the resulting scaling law one easily deduces $\overline{\langle x(t)\rangle^2} \sim \ln^4 t$, the law for Sinai diffusion, Eq.(6). These results for $N(\epsilon)$ and $\langle \pi_k(t)\rangle$ should be contrasted with the behavior for maps or random walks generating normal diffusion, for which one obtains $\langle \pi_k(t)\rangle \sim t^{-1/2}$ and $N(\epsilon) \sim \epsilon^{1/2}$.

The diffusive behavior of dynamical systems was recently related to escape rates from regions in state space (see "escape rate formalism" in [4] [3] and refs. therein). To be more specific, one finds that the escape from a region of size L is described by an escape rate $\gamma(L)$, which decreases for large L as $\gamma(L) \sim D(\chi/L)^2$ with D being the diffusion constant and χ a geometric factor. Conversely $D = \lim_{L\to\infty} \gamma(L) L^2/\chi^2$. Since we have shown in Section 2 that D vanishes for the considered disordered maps, $\gamma(L)$ must vanish faster than L^{-2} with increasing system size, and one wonders how. To investigate this question we may again exploit the connection between our dynamical systems and Markov models. Further we are going to use that escape rates are determined by the maximal eigenvalue of suitably chosen matrices [4].

We consider first a semi-infinite random chain of maps of Sinai type as in Fig.2, or equivalently, the semi-infinite tridiagonal Markov transition matrix $\mathbf{P}$ with a reflecting boundary condition at cell $i = 1$ and otherwise with matrix elements as above in Eq.(13). Define the $(L \times L)$-submatrix $\mathbf{Q}$ of the matrix $\mathbf{P}$, which is obtained by considering only transitions connecting the states $i = 1, 2, \ldots, L$. The matrix $\mathbf{Q}$ is no longer stochastic but sub-stochastic, i.e. the still positive entries of at least one row no longer add up to one, but $\sum_j Q_{ij} < 1$ for some i. Therefore its largest eigenvalue $\lambda^{(1)}$ is strictly smaller than 1. If one chooses an initial distribution in the segment S containing cells $\{1, 2, \ldots, L\}$ and asks for the fraction still to be found in S after t iterations (without considering returns to S from outside), one finds that it decays asymptotically as $\left(\lambda^{(1)}\right)^t \equiv \exp(-\gamma t)$. This is easily established by defining the states $i = L+1$, $L+2$, etc. as absorbing states and by considering the spectral decomposition of $\mathbf{Q}$ analogous to Eq.(14). We can thus pick one realization of the disordered chain of maps and within this realization we increase the segment length L and correspondingly the dimension of the submatrix $\mathbf{Q}$. Diagonalizing $\mathbf{Q}$ for each L and taking the maximal eigenvalue $\lambda^{(1)}(L)$ yields the length dependence of the escape rate as $\gamma(L) = -\ln(\lambda^{(1)}(L))$. The result of such a procedure where L was increased in steps of $\Delta L = 1$ up to $L_{\max} = 200$ is depicted in Fig.7(a).

In Fig.7(a) one finds an irregular increase of $\gamma(L)$ with a trend given roughly

Fig. 7. a) The dependence of $-\ln\gamma(L)$ on the length L in a doubly logartithmic plot. The system parameters are as in Fig.5. b) The same as in a) but averaged over 10 disorder realizations. The dashed line corresponds in both graphs to the functional form $\widetilde{\gamma}(L) = a\exp(-bL^{1/2})$ with constants a and b.

by the dashed line. This trend is confirmed in the averaged escape rate $\overline{\gamma(L)}$ of Fig.7(b). Its decay as a stretched exponential

$$\overline{\gamma(L)} = a\exp(-bL^{\beta}) \tag{21}$$

with exponent $\beta = 1/2$ is consistent with the picture of a random landscape where the barriers increase with the system length as $L^{1/2}$ as discussed in connection with Eq.(4). It is also consistent with the result of Noskovicz and Goldhirsch [67], who found for the Sinai model that the *typical* mean first passage time τ, and thus $1/\gamma$, depends on L as $\ln\tau \sim L^{1/2}$.

4.2 Maps with topological disorder

In the following we will show that the picture we developed for maps with Sinai disorder has to be modified for Markov maps with topological disorder (see Fig.1(a)). The first indication of deviations from the Sinai case is seen in the $L-$dependence of the escape rates. They were again obtained by calculating the maximal eigenvalue of the corresponding $(L \times L)$-submatrices $\mathbf{Q}$. The Fig.8(a) is analogous to Fig.7(b), but for the system of Fig.1(a).

In the log-log plot of $\left|\ln\overline{\gamma(L)}\right|$ vs. L one finds again a linear behavior, but in contrast to Fig.7(b) where we found a slope $\beta = 1/2$, we now find $\beta \simeq 0.34$. This exponent is confirmed in Fig.1(b), where we extend the range up to $L = 1024$ choosing fewer $L-$values equidistant on a logarithmic scale and apply a different sampling strategy. The exponent β was obtained here from a least-squares fit of points with $L \geq 32$. Thus the escape from segments of length L follows again a stretched exponential, i.e. $\overline{\gamma(L)} = a\exp(-bL^{0.34})$, but due to the larger exponent β it is faster than in the Sinai case. Using the escape rate formalism [4] this result implies that the Kolmogorov-Sinai entropy $h_{KS}(L)$ of the dynamics on the fractal repeller within a finite segment

Fig. 8. a) The dependence of $-\ln\overline{\gamma(L)}$ on the length L for the disordered map of Fig.1 in a doubly logartithmic plot. As in Fig. 7(b) it was obtained by averaging over 10 disorder realizations ($L_{\max} = 300$). b) The same as in a) but for larger systems ($L \leq 1024$) and every data point representing an average over 50 different disorder realizations (in total 400 different systems). The coarsely dashed line corresponds in both graphs to the asymptotic form $\widetilde{\gamma}(L) = a\exp(-bL^{\beta})$ with $\beta \simeq 0.34$. For comparison the Sinai behavior, i.e. $\beta \simeq 1/2$, is shown in (b).

L typically deviates from its asymptotic infinite L value $h_{KS}(L=\infty) = \ln 4$ exactly by $\overline{\gamma(L)}$.

We have seen in the system with Sinai disorder that the exponent $\delta = 2$, which characterizes the logarithmic decay of the return probability $\langle \pi_k(t) \rangle \propto 1/\left|\ln t\right|^{\delta}$, was the inverse of β, i.e. $\delta = 1/\beta$. The heuristics behind this connection is that both the escape from a segment and the decay of probability in the initial cell are mediated by the same mechanism for the anomalous drift in the system. From such a reasoning one expects that in the system with topological disorder the spectrum of the propagator and correspondingly the density of relaxation rates is also different from the Sinai case. First we note that now the spectrum is no longer real, since the transition matrix is no longer tridiagonal due to the coupling to next-nearest neighbor cells. The spectrum obtained from diagonalizing $\mathbf{P}$ as in Eq.(14) is shown in Fig.9(a).

Fig. 9. a) The spectrum in the complex plane of the transition matrix corresponding to the topologically disordered map of Fig.1 ($L = 2000$ cells). The eigenvalues with $\mathrm{Re}\,\lambda > 0$ have zero imaginary part, i.e. are purely real. b) The eigenvalues ordered according to their real part. The clustering of the real eigenvalues near $\lambda = 1$ give rise to a singularity in the density of relaxation rates (see Fig.10).

The part of the spectrum near $\lambda = 1$ (see Fig.9(b)), which is purely real

and which determines the long time behavior, again appears to produce a singularity in the density of relaxation rates. This is confirmed in the plot of the integrated density N vs. $|\ln \epsilon|$ on a doubly logarithmic scale as shown in Fig.10.

Fig. 10. Doubly logarithmic plot of the integrated density of relaxation rates N vs. $|\ln \epsilon|$ (averaged over 50 disorder realizations of length $L = 2000$) for topological disorder near $\epsilon = 0$. The dashed line corresponds to a behavior $N(\epsilon) \sim 1/|\ln \epsilon|^{2.6}$.

We find again a behavior near the band edge of the form Eq.(20) but now with an exponent $\delta \simeq 2.6$. The relation $\beta = 1/\delta$, which is valid for the Sinai case, is only roughly fulfilled ($\beta = 0.34$ vs. $1/\delta \simeq 0.38$), but this may be due numerical inaccuracies in determining the exponents. In any case this means that the anomalous drift in the topologically disordered system is determined by other mechanisms than in the Sinai case. The reason seems to lie in the following observation. For Sinai disorder and also its continuum limit the stationary distribution for finite systems do not carry probability currents due to detailed balance. This had let to density fluctuations of the order $O(\exp a\sqrt{L})$. In contrast, the topologically disordered systems with its transitions to next-nearest cells do support currents also in the stationary state. This is also the reason, why there exists no simple expression for the stationary distribution in this case. On the other hand, numerical investigations (not shown here) of the "ground state" indicate that also in this case the stationary density behaves as in the Sinai case under changes of the system length L, i.e. $\ln \rho \simeq L^{1/2}$. The existence of currents in the stationary state, however, prohibits an interpretation of the state dynamics as activated process in a potential as it was possible in the Sinai case. This fact appears to be responsible also for the modified anomalous drift properties for systems with transitions to next-nearest cells. The latter system obviously is not in the same class as the system with Sinai disorder, although it shows the same boundedness of the mean-square displacement $\sigma^2(t) = \langle x_t^2 \rangle - \langle x_t \rangle^2$, at least numerically (Fig.1(b)).

5 Further Generalizations and Perspectives

The system with topological disorder can be regarded as special case of maps with disorder which transfer points $x(t)$ into next-nearest cells. For these more

general maps there may exist in the piecewise linear case again a Markov partition made up by the integer intervals. Such Markov maps are similar to that of Fig.2, but now with five instead of three branches in each unit cell. The corresponding Markov models are random walks with next-nearest neighbor transitions. Analogously maps with even farther reaching transitions may be defined, which correspond to random walks with next-next-nearest neighbor transitions, etc. A new aspect shows up, however, already for Markov maps with transitions to next-nearest cells. At each site i one has the freedom to fix independently four transition probabilities $\mathbf{p}_i \equiv \{p_{i,i-2}, p_{i,i-1}, p_{i,i+1}, p_{i,i+2}\}$ (or slopes), p_{ii} follows by normalization. The first fundamental problem is to decide whether the resulting random system has a bias or not. In mathematical terms this amounts to the question of recurrence of the random walk, i.e. what is the generalization of the Sinai condition $\overline{\ln(p_{i,i-1}/p_{i,i+1})} = 0$. There exists an answer in terms of the Lyapunov spectrum of a certain infinite product of random matrices $\left\{\mathbf{A}^{(i)}\right\}$ associated with such a random environment, which was provided by Key [68] (see Appendix). Already for Markov maps with transitions to next-nearest cells, however, one needs to calculate the Lyapunov spectrum of an infinite product of random (4×4)-matrices, which cannot in general be done analytically. Thus one does in general not know exactly whether one is in a bias-free system. There are, however, special cases for which a vanishing bias is guaranteed. Such a situation is given e.g. by the following generalization of binary disorder: Take two sets of transition probabilities $\mathbf{p} \equiv \{p_{i-2}, p_{i-1}, p_{i+1}, p_{i+2}\}$ and $\overline{\mathbf{p}} \equiv \left\{\overline{p}_{i-2}, \overline{p}_{i-1}, \overline{p}_{i+1}, \overline{p}_{i+2}\right\} = \{p_{i+2}, p_{i+1}, p_{i-1}, p_{i-2}\}$, i.e. $\overline{\mathbf{p}}$ maps points in the same manner say to the left (right) as does $\mathbf{p}$ to the right (left). If one defines a random environment by randomly sampling $\mathbf{p}_i$ with equal probability from $\{\mathbf{p},\overline{\mathbf{p}}\}$ the resulting system obviously has no bias by symmetry. Such a system is a generalization of the Sinai system with binary disorder, where $\mathbf{p}_i \equiv \{p_{i,i-1}, p_{i,i+1}\}$ is with equal probability taken e.g. as $\mathbf{p} = \{1/9, 8/9\}$ and $\overline{\mathbf{p}} = \{8/9, 1/9\}$ as we did for calculating the spectrum of Fig.5. We calculated escape rates, spectra, and integrated densities of relaxation rates also for such disordered systems with binary disorder and transitions to next-nearest neighbors. E.g. for $\mathbf{p} \equiv \{1/6, 1/6, 1/6, 1/3\}$ and correspondingly $\overline{\mathbf{p}} \equiv \{1/3, 1/6, 1/6, 1/6\}$ we found again the stretched exponential in the escape rates and the logarithmic decay of the return probability, this time with exponents $\beta \simeq 0.24$ (average over 500 disorder realizations) and $\delta \simeq 3.0$, respectively. Thus we find again new exponents, where in addition the relation $\beta = 1/\delta$ seems to be violated even more drastically. A systematic investigation of the dependence of these exponents on the transition range and other parameters is currently in progress. We finally should mention that the more general binary disorder introduced above can be generalized easily to smoothly varying nonlinear maps. An example is the sinusoidal variation within the cells as investigated in [30], where the localization property was also observed. The anomalous drift behavior appears to be more subtle and deserves further investigations.

Acknowledgement: I thank the organizers of the Conference on "Microscopic Chaos and Transport in Many-Particle Systems" for giving me the opportunity to present these results and M. Gundlach for pointing me to the work of E. Key [68]. I also thank the anonymous referees for their constructive remarks.

6 Appendix

Here we briefly restate in terms of Markov maps a criterion by Key [68], which guarantees recurrence of the associated random walk, i.e. a bias-free situation. Consider a random walk with transitions up l neighbors to the left and r neighbors to the right. Define at each site the $(r+l)$-dimensional vector of transition probabilities $\mathbf{p}_i \equiv \{p_{i,i-l}, \ldots, p_{i,i-1}, p_{i,i+1}, \ldots, p_{i,i+r}\}$. For the theorem to hold the $\{\mathbf{p}_i\}$ defining the random environment must be i.i.d. Furthermore one requires $\overline{\ln p_{i,i-l}} > -\infty$, $\overline{\ln p_{i,i+r}} > -\infty$, and $p_{i,i-l} \neq 0$ and $p_{i,i+r} \neq 0$ at all sites i. So our topologically disordered map of Fig.1 does not belong to the models where the theorem holds. One associates to each site i a $(l+r) \times (l+r)$ matrix $\mathbf{A}^{(i)}$ with elements

$$A^{(i)}_{mn} = \delta_{m,n-1} + \delta_{m,l+r} \frac{\delta_{n,r+1} - p_{i,i+r+1-n}}{p_{i,i-l}} \tag{22}$$

which is built from elements of the vector $\mathbf{p}_i$. As an example, for next-nearest neighbor models as discussed in Section 5 with $l = r = 2$ the (4×4) matrices $\left\{\mathbf{A}^{(i)}\right\}$ are given by

$$\mathbf{A}^{(i)} = \begin{pmatrix} 0 & 1 & 0 & 0 \\ 0 & 0 & 1 & 0 \\ 0 & 0 & 0 & 1 \\ \frac{-p_{i,i+2}}{p_{i,i-2}} & \frac{-p_{i,i+1}}{p_{i,i-2}} & \frac{1-p_{i,i}}{p_{i,i-2}} & \frac{-p_{i,i-1}}{p_{i,i-2}} \end{pmatrix} \tag{23}$$

Since the $\{\mathbf{p}_i\}$ must be i.i.d., this holds also for the matrices $\left\{\mathbf{A}^{(i)}\right\}$. The criterion of Key states that the random walk in the random environment given by the $\{\mathbf{p}_i\}$ is recurrent, if for the infinite product of random matrices $\mathbf{A}^{(-L)} \cdot \ldots \cdot \mathbf{A}^{(-3)} \cdot \mathbf{A}^{(-2)} \cdot \mathbf{A}^{(-1)} \cdot \mathbf{A}^{(0)}$, $L \to \infty$, the Lyapunov exponents of this product fulfill the condition $\lambda_r = \lambda_{r+1} = 0$, where the ordering of the Lyapunov exponents is $\lambda_1 \leq \lambda_2 \leq \ldots \leq \lambda_{l+r}$. Since it can be shown that one of the exponents λ_r or λ_{r+1} is zero anyway, this is a condition for one more Lyapunov exponent in the spectrum. Key constructs special classes of

systems with $l+r=3$ and $l+r=4$ where $\lambda_r = \lambda_{r+1} = 0$, which can easily be translated to dynamical systems of piecewise linear maps by the prescription Eq.(13). For systems with binary disorder, as introduced in Section 5, one associates to the vectors $\mathbf{p}$ and $\overline{\mathbf{p}}$ matrices $\mathbf{A}$ and $\overline{\mathbf{A}}$, respectively. One can show that $\overline{\mathbf{A}}$ can be expressed by $\mathbf{A}$ as $\overline{\mathbf{A}} = \mathbf{I} \cdot \mathbf{A}^{-1} \cdot \mathbf{I}$, where $\mathbf{I}$ inverts indices, i.e. $I_{mn} = \delta_{m,l+r+1-n}$. These systems with binary disorder are not contained in Key's special classes. Conversely one can conclude that from symmetry considerations it follows that products of random matrices containing $\mathbf{A}$ and $\overline{\mathbf{A}}$ (with $l = r$) with equal probability have two vanishing Lyapunov exponents in the center of their Lyapunov spectrum. Generalizations of this statement to products with several matrices $\mathbf{A}, \mathbf{A}', \mathbf{A}'', \ldots$ and the corresponding $\overline{\mathbf{A}}, \overline{\mathbf{A}}', \overline{\mathbf{A}}''$, etc. are obvious.

References

[1] H. G. Schuster, Deterministic Chaos, 3rd augm. ed. (VCH, Weinheim, 1995).

[2] E. Ott, *Chaos in Dynamical Systems.* (Cambridge University Press, Cambridge, 1993).

[3] J.R. Dorfman, *An Introduction to Chaos in Nonequilibrium Statistical Mechanics.* (Cambridge University Press, Cambridge, 1999).

[4] P. Gaspard, *Chaos, Scattering and Statistical Mechanics.* (Cambridge University Press, Cambridge, 1998).

[5] M. Mezard, G. Parisi and M.A. Virasoro, *Spin glass theory and beyond* (World Scientific, Singapore,1987).

[6] see e.g.: H. van Beijeren and J. R. Dorfman, Phys. Rev. Lett. **74**, 4412 (1995); and refs. therein.

[7] D. Weiss et al., Phys. Rev. Lett. **66**, 2790 (1991).

[8] R. Fleischmann, T. Geisel and R. Ketzmerick, Phys. Rev. Lett. **68**, 1367 (1992).

[9] T. Geisel, A. Zacherl and G. Radons, Phys. Rev. Lett. **59**, 2503 (1987).

[10] T. Geisel and J. Nierwetberg, Phys. Rev. Lett. **48**, 7 (1982).

[11] S. Grossmann and H. Fujisaka, Phys. Rev. A **26**, 1779 (1982).

[12] H. Fujisaka and S. Grossmann, Z. Phys. B **48**, 261 (1982).

[13] M. Schell, S. Fraser and R. Kapral, Phys. Rev. A **26**, 504 (1982).

[14] T. Geisel and S. Thomae, Phys. Rev. Lett. **52**, 1936 (1984).

[15] T. Geisel, J. Nierwetberg and A. Zacherl, Phys. Rev. Lett. **54**, 616 (1985).

[16] R. Artuso, Phys. Lett. A **202**, 195 (1992).

[17] G. Zumofen and J. Klafter, Phys. Rev. E **47**, 851 (1993).

[18] X.-J. Wang and C.-K. Hu, Phys. Rev. E **48**, 728 (1993).

[19] R. Artuso, G. Casati and R. Lombardi, Phys. Rev. Lett. **71**, 62 (1993).

[20] R. Stoop, Phys. Rev. E **49**, 4913 (1994).

[21] R. Klages and J. R. Dorfman, Phys. Rev. Lett. **74**, 387 (1995).

[22] G. Radons, Phys. Rep. **290**, 67 (1997).

[23] C. Beck and F. Schlögl, *Thermodynamics of Chaotic Systems* (Cambridge University Press, Cambridge, 1993).

[24] J.-P. Bouchaud and A. Georges, Phys. Rep. **195**, 127 (1990).

[25] Ya. G. Sinai, Theor. Prob. Appl. **27**, 247 (1982).

[26] A. Golosov, Commun. Math. Phys. **92**, 491 (1984).

[27] Although $\sigma^2(t)$ typically remains finite for all times t, averaging $\sigma^2(t)$ over the random environments leads to a divergence for $t \to \infty$, i.e. $\lim_{t\to\infty} \overline{\sigma^2(t)} = \infty$, due to rare contributions from atypical configurations of the environment [52] [53]. This is an example for the difference between typical values and their mean encountered often in disordered systems.

[28] The initial increase and subsequent decrease of $\sigma^2(t)$ seen in Fig.1b can be understood in terms of a relaxation process of the initial distribution into a first local trap of the system. In the case of the Sinai systems this process has been visualized in Fig.4 of Ref.[52].

[29] B.D. Hughes, *Random Walks and Random Environments*, Vol.2: Random Enironments, Chap.6 (Clarendon Press, Oxford, 1996).

[30] G. Radons, Phys. Rev. Lett. **77**, 4748 (1996).

[31] G. Radons, Adv. Solid State Physics / Festkörperprobleme **38**, 439 (1999).

[32] E. Hopf, *Ergodentheorie* (Springer, Berlin, 1937).

[33] B. Derrida and Y. Pomeau, Phys. Rev. Lett. **48**, 627 (1982).

[34] B. Derrida, J. Stat. Phys. **31**, 433 (1983).

[35] G. Radons, J. Phys. A **31**, 4141 (1998).

[36] P. Jung, J.G. Kissner and P. Hänggi, Phys. Rev. Lett. **76**, 3436 (1996).

[37] Th. Harms and R. Lipowsky, Phys. Rev. Lett. **79**, 2895 (1997).

[38] E. Barkai and J. Klafter, Phys. Rev. Lett. **79**, 2245 (1997).

[39] L. Lundgren et al., Phys. Rev. Lett. **51**, 911 (1983).

[40] L.C.E. Struik, *Physical Aging in Amorphous Polymers and other Materials* (Elsevier, Amsterdam, 1978).

[41] M. Rubí and C. Pérez-Vicente (eds.), *Complex Behaviour in Glassy Systems* (Springer, Berlin, 1997).

[42] J.P. Bouchaud, L.F. Cugliandulo, J. Kurchan and M. Mezard, in: A.P. Young (ed.), *Spin Glasses and Random Fields* (World Scientific, Singapore, 1998), cond-mat/9702070.

[43] E. Vincent, et al., in: [41], p.184, cond-mat/9607224.

[44] E. Marinari and G. Parisi, J. Phys. A **26**, L1149 (1993).

[45] F. Ritort, Phys. Rev. Lett. **75**, 1190 (1995).

[46] L. Laloux and P. Le Doussal, Phys. Rev. E **57**, 6296 (1998).

[47] D.S. Fisher, P. Le Doussal and C. Monthus, Phys. Rev. Lett. **80**, 3539 (1998).

[48] P. Le Doussal, C. Monthus and D.S. Fisher, Phys. Rev. E **59**, 4795 (1999).

[49] L.F. Cugliandulo, J. Kurchan and G. Parisi: J.Phys. I France **4,** 1641 (1994).

[50] E. Barkai, Phys. Rev. Lett. **90**, 104101 (2003).

[51] J. Dräger and J. Klafter, Phys. Rev. Lett. **84**, 5998 (2000).

[52] J. Chave and E. Guitter, J. Phys. A **32**, 445 (1999).

[53] C. Monthus and P. Le Doussal, Phys. Rev. E **65**, 066129 (2002).

[54] S.N. Majumdar and A. Comtet, Phys. Rev. E **66**, 061105 (2002).

[55] C. Monthus, Localization properties of the anomalous diffusion phase $x \sim t^{\mu}$ in the directed trap model and in the Sinai diffusion with bias. cond-mat/0212212.

[56] C. Monthus and P. Le Doussal, Energy dynamics in the Sinai model. cond-mat/0206035.

[57] J. Heldstab, H. Thomas, T. Geisel and G. Radons, Z. Phys. B **50**, 141 (1983).

[58] S. Grossmann, Z. Phys. B **57**, 77 (1984).

[59] M. Bianucci, R. Manella, X. Fan, P. Grigolino and B.J. West, Phys. Rev. E 47, 1510 (1993).

[60] M. Bianucci, R. Manella, B.J. West and P. Grigolino, Phys. Rev. E 50, 2693 (1994).

[61] I.S. Gradshteyn and I.M. Ryzhik, *Tables of Integrals, Series, and Products, 6th ed.* (Academic Press, San Diego, 2000).

[62] I.M. Lifshits, S.A. Gredeskul and L.A. Pastur, *Introduction to the theory of disordered systems* (Wiley, New York, 1988)

[63] H. Risken, *The Fokker-Planck Equation, 3rd ed.* (Springer, Berlin, 1996).

[64] J.P. Bouchaud, A. Comtet, A. Georges and P. Le Doussal, Europhys. Lett. **3**, 653 (1987).

[65] T. Schneider, A. Politi and R. Badii, Phys. Rev. A **34**, 2505 (1986).

[66] M. Nauenberg, J. Stat. Phys. **41**, 803 (1985).

[67] S.H. Noskowicz and I. Goldhirsch, Phys. Rev. A **42**, 2047 (1990).

[68] E.S. Key, Ann. Probab. **12**, 529 (1984).

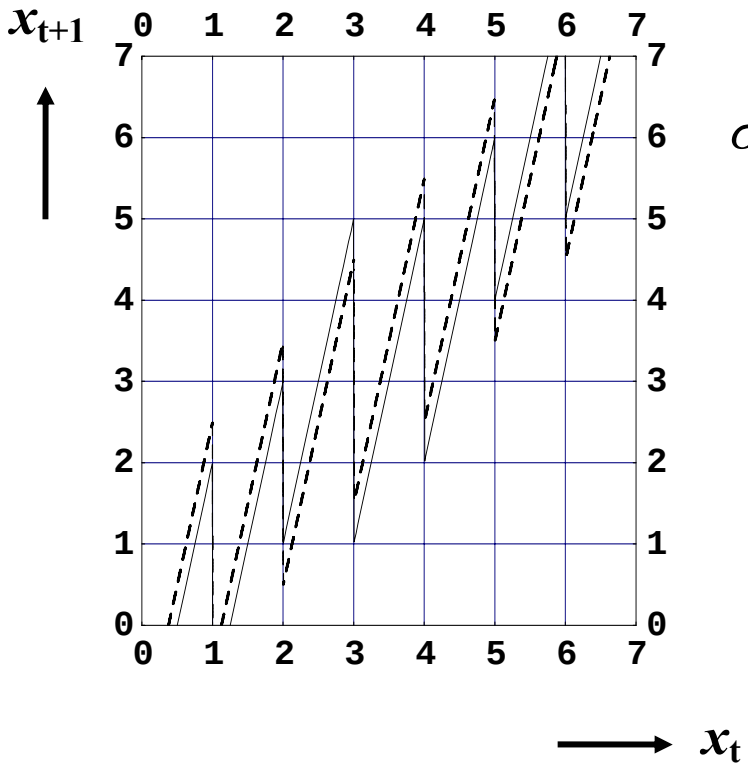

(a)

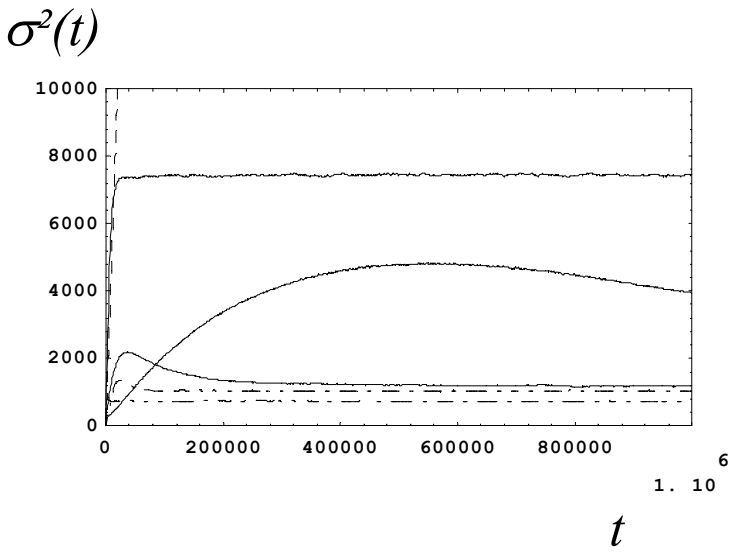

(b)

Physica D / Radons / Fig.1

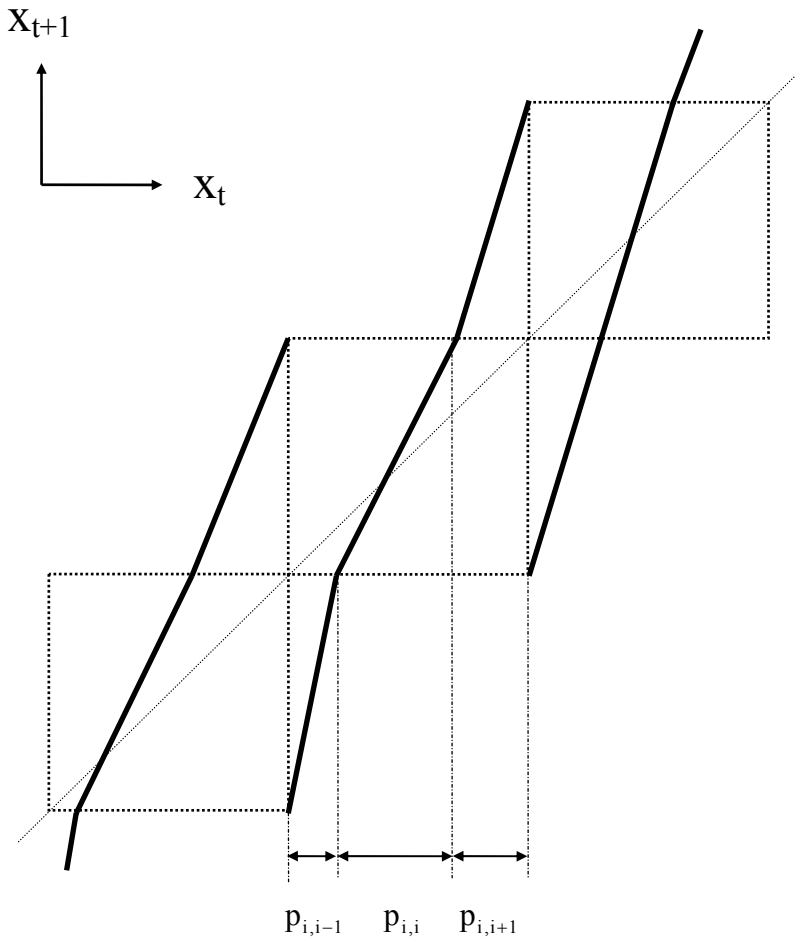

Physics D / Radons / Fig.2

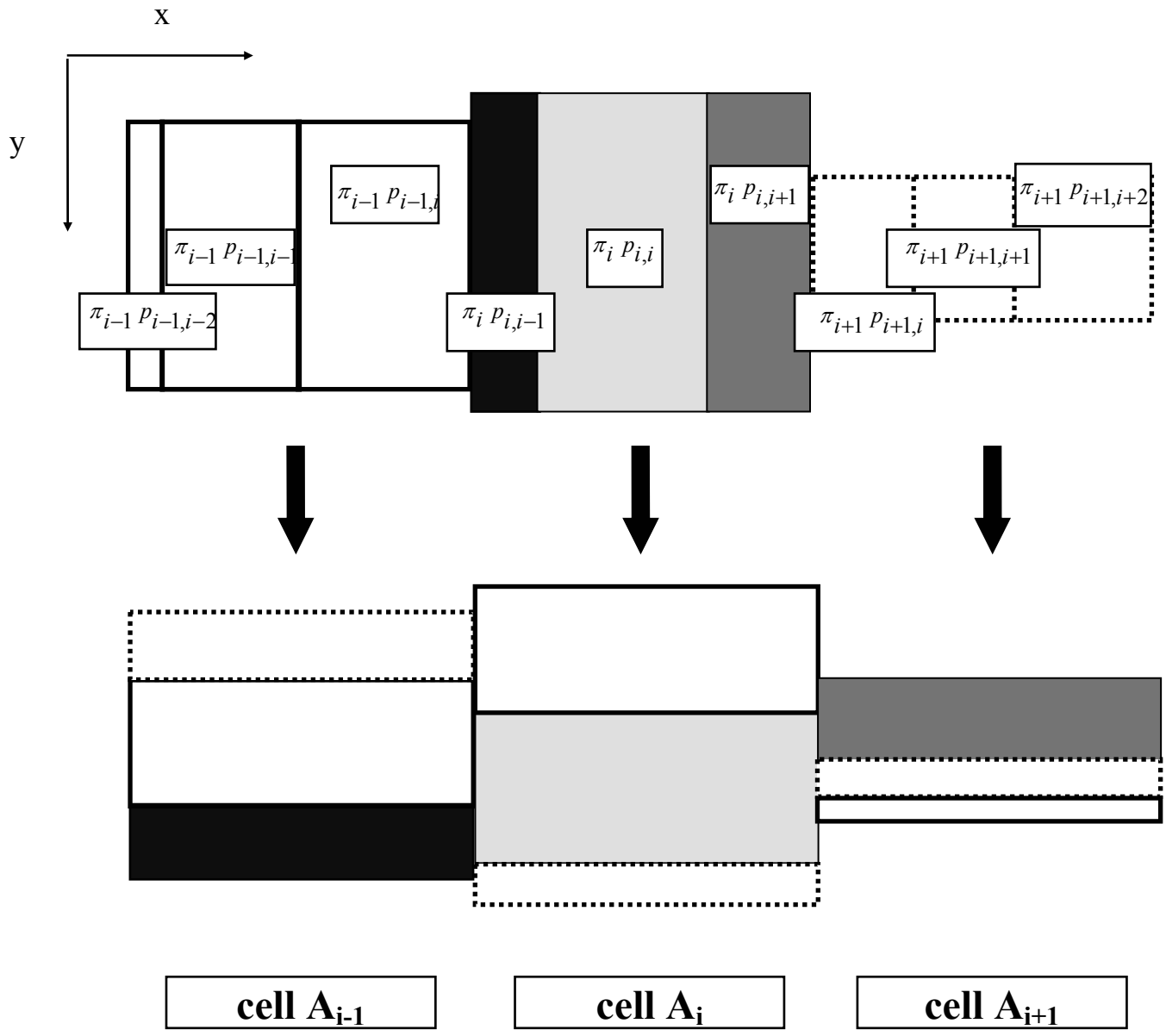

Physica D / Radons / Fig.3

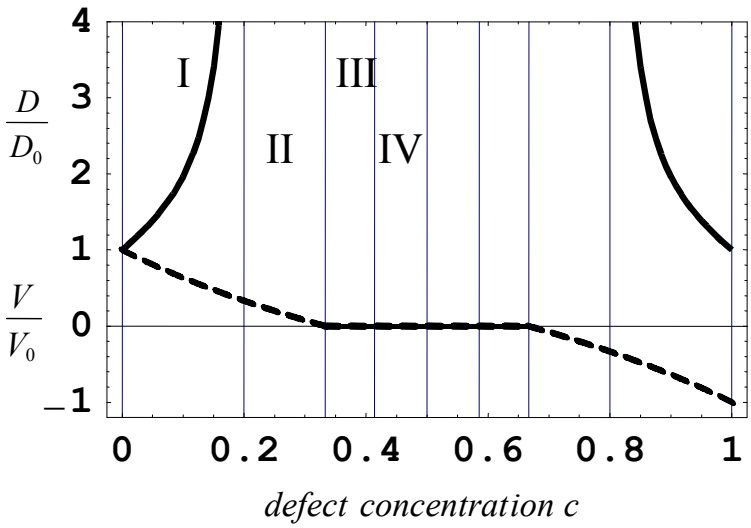

Physica D / Radons / Fig.4

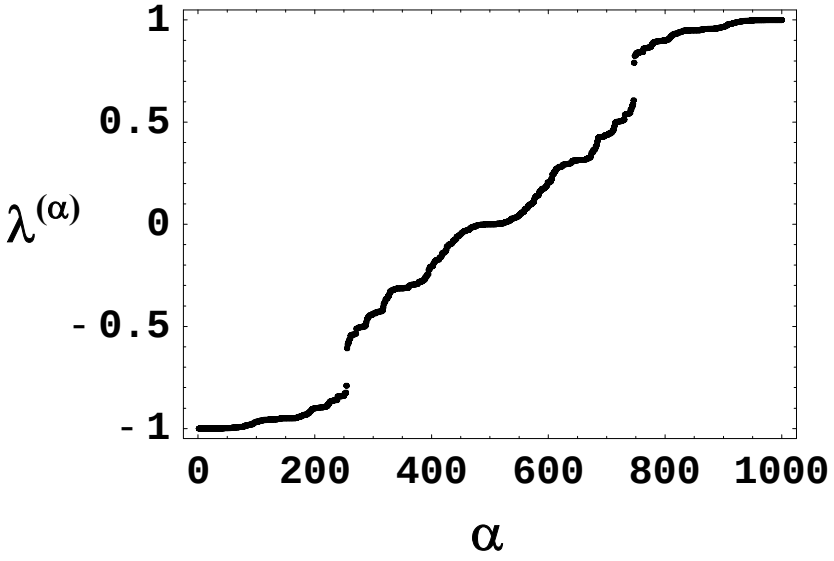

Physica D / Radons / Fig.5

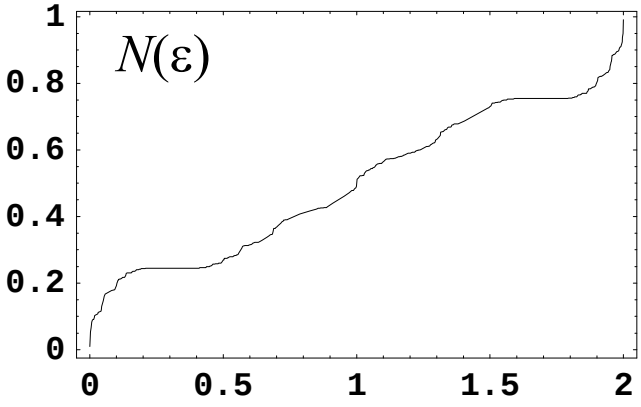

(a)

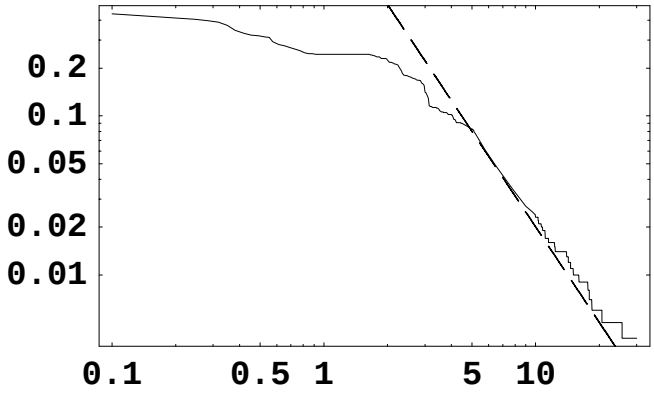

(b)

Physica D / Radons / Fig.6

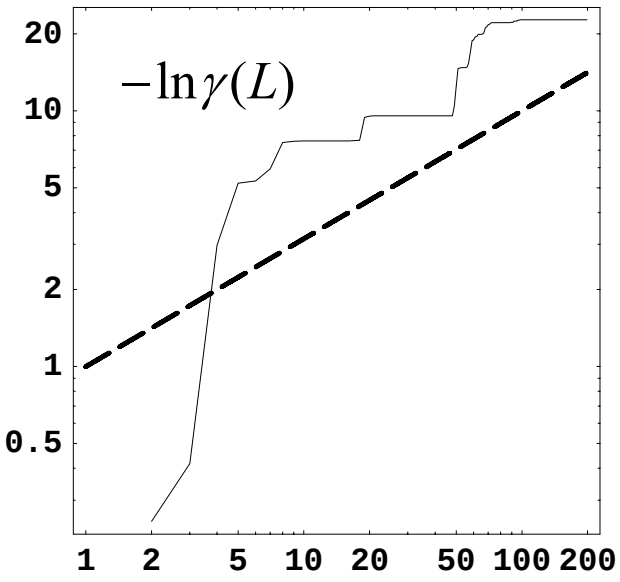

(a)

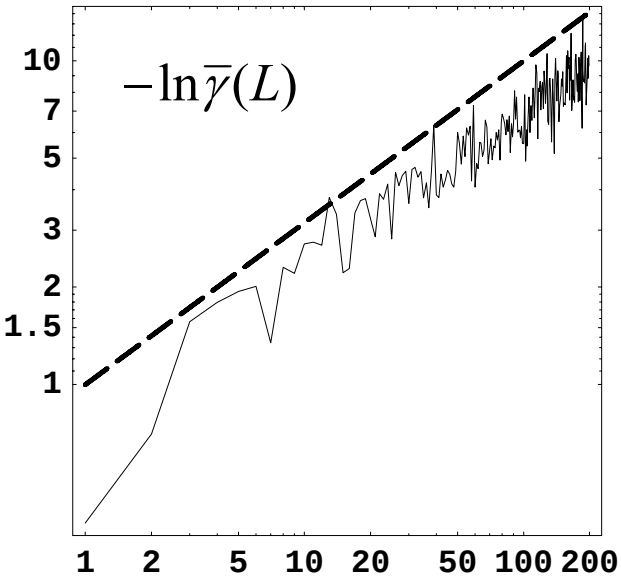

(b)

Physica D / Radons / Fig.7

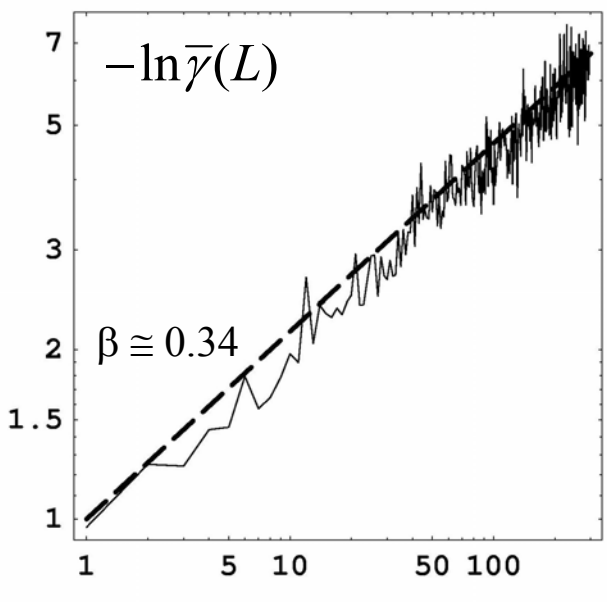

(a)

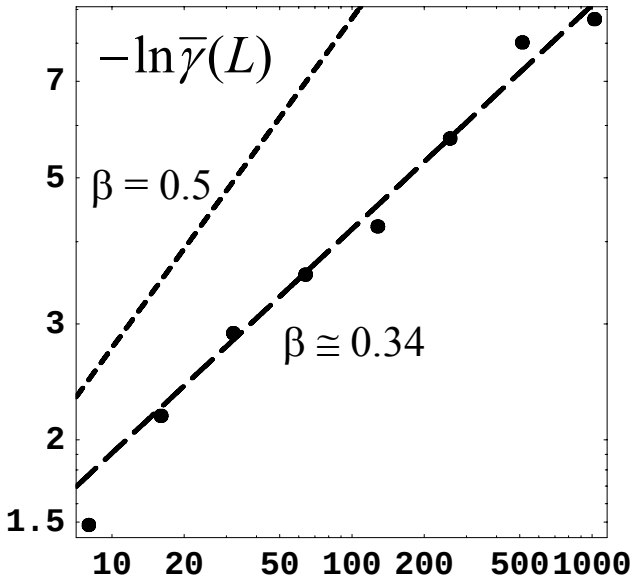

(b)

Physica D / Radons / Fig.8

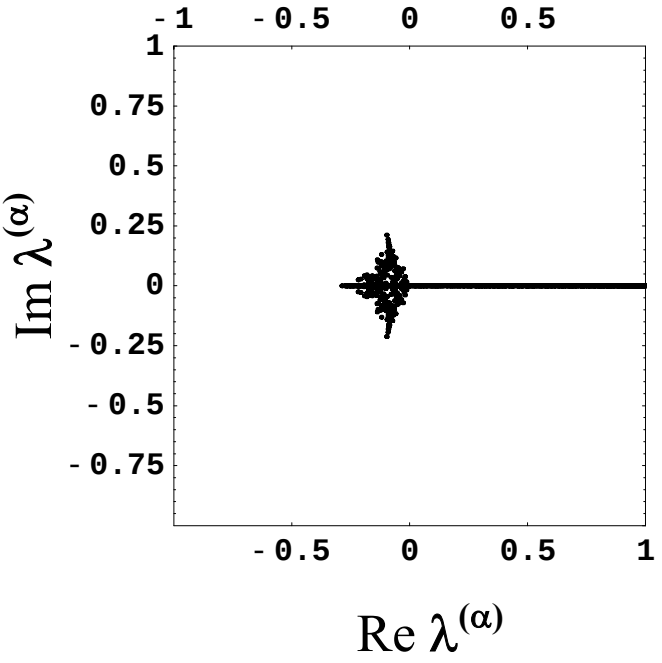

(a)

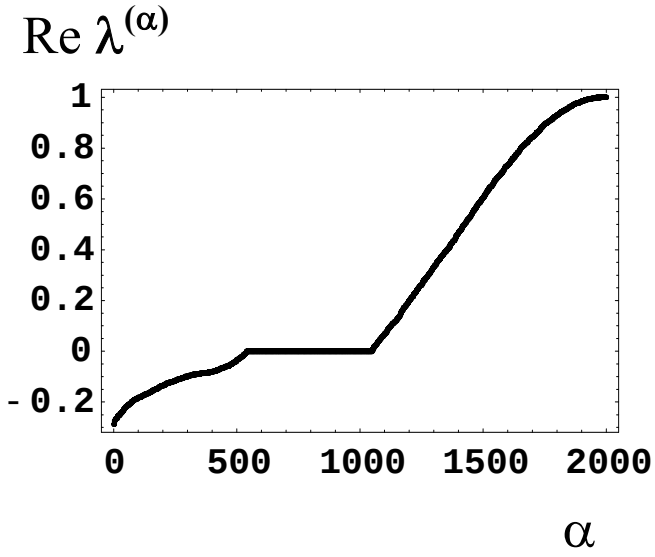

(b)

Physica D / Radons / Fig.9

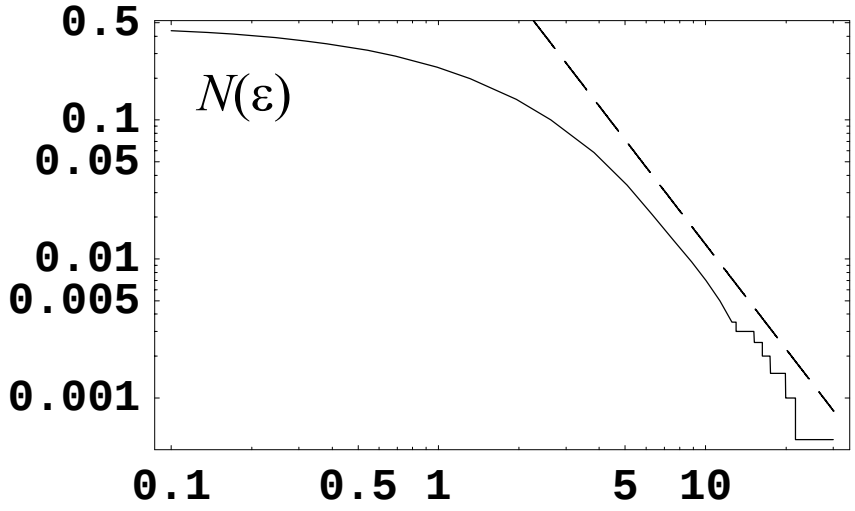

Physica D / Radons / Fig.10